

Graphoepitaxy of High-Quality GaN Layers on Graphene/6H–SiC

András Kovács,* Martial Duchamp, Rafal E. Dunin-Borkowski, Rositza Yakimova, Péter L. Neumann, Hannes Behmenburg, Bartosz Foltynski, Cristoph Giesen, Michael Heuken, and Béla Pécz*

The implementation of graphene layers in gallium nitride (GaN) heterostructure growth can solve self-heating problems in nitride-based high-power electronic and light-emitting optoelectronic devices. In the present study, high-quality GaN layers are grown on patterned graphene layers and 6H–SiC by metalorganic chemical vapor deposition. A periodic pattern of graphene layers is fabricated on 6H–SiC by using polymethyl methacrylate deposition and electron beam lithography, followed by etching using an Ar/O₂ gas atmosphere. Prior to GaN growth, an AlN buffer layer and an Al_{0.2}Ga_{0.8}N transition layer are deposited. The atomic structures of the interfaces between the 6H–SiC and graphene, as well as between the graphene and AlN, are studied using scanning transmission electron microscopy. Phase separation of the Al_{0.2}Ga_{0.8}N transition layer into an AlN and GaN superlattice is observed. Above the continuous graphene layers, polycrystalline defective GaN is rapidly overgrown by better quality single-crystalline GaN from the etched regions. The lateral overgrowth of GaN results in the presence of a low density of dislocations ($\approx 10^9 \text{ cm}^{-2}$) and inversion domains and the formation of a smooth GaN surface.

properties,^[1] which are highly desirable for numerous applications. Graphene has a very high heat conductivity^[2] of up to 5000 W mK⁻¹, suggesting that it may be a suitable candidate for solving self-heating problems in nitride-based (e.g., GaN, InGaN, and AlGaN) high-power electronics^[3] and solid state optoelectronics.^[4] High-quality epitaxial nitride layers can be grown on single-crystalline substrates, such as ZnO, SiC, and Al₂O₃ (sapphire), using intermediate buffer and transition layers. The lack of chemical reactivity between GaN (or AlN as a buffer) and graphene leads to imperfect polycrystalline growth, resulting in a large number of undesired defects in the GaN and a possible rough surface, making the integration of graphene into nitride thin film heterostructures very challenging. In order to overcome the growth issue, Han and co-workers^[5] used lithographically patterned graphene oxide to

1. Introduction

Graphene has attracted tremendous attention over the past few years because of its 2D atomic structure and unique physical

improve heat dissipation in light-emitting diodes (LEDs). Chung et al.^[6] used a ZnO coating on O₂ plasma-treated graphene layers to grow high-quality GaN layers and to make the resulting heterostructure transferable to any substrate. Yan et al.^[7] implemented thermal heat-escaping channels from graphene layers on top of AlGaN/GaN transistors deposited on SiC.

Dr. A. Kovács, Dr. M. Duchamp,
Prof. R. E. Dunin-Borkowski
Ernst Ruska-Centre for Microscopy and Spectroscopy
with Electrons and Peter Grünberg Institute
Forschungszentrum Jülich
52425 Jülich, Germany
E-mail: a.kovacs@fz-juelich.de



Prof. R. Yakimova
Department of Physics
Chemistry and Biology
Linköping University
581 83, Linköping, Sweden

P. L. Neumann, Prof. B. Pécz
Institute for Technical Physics and Materials Science
Research Centre for Natural Sciences
Hungarian Academy of Sciences
P.O. Box 49, H-1525, Budapest, Hungary
E-mail: pecz@mfa.kfki.hu

Dr. H. Behmenburg, B. Foltynski, Dr. C. Giesen, Prof. M. Heuken
AIXTRON SE
Kaiserstrasse 98, 52134, Herzogenrath, Germany

In the present study, we show that a *c*-axis-oriented GaN layer that has high structural perfection can be grown by metalorganic chemical vapor deposition on patterned graphene layers and (0001) oriented 6H–SiC using an AlN buffer and Al_{0.2}Ga_{0.8}N transition layers. The nucleation and growth of the heterostructure are studied using advanced transmission electron microscopy (TEM) in cross-sectional geometry. The GaN layer is observed to have a smooth surface and an estimated dislocation density of $3 \times 10^9 \text{ cm}^{-2}$, which is in the same range as the dislocation density in a control sample grown without graphene layers. We show that the GaN that is formed above the continuous graphene is polycrystalline and is overgrown laterally by single-crystalline GaN.

2. Results and Discussion

2.1. Etching of Graphene and Nitride Deposition

Graphene layers were prepared on the Si-terminated face of an 0001-oriented 6H–SiC single crystal 2 in. wafer by

a high-temperature sublimation process^[8] developed at Linköping University. Auger electron spectroscopy,^[9] was used to determine that the number of graphene layers was usually 2–3, with small regions containing up to ten graphene layers. The continuous graphene layers were covered with polymethyl methacrylate (PMMA) and patterned using electron beam lithography, to leave 1 μm wide unmasked areas in a 3 μm periodic pattern, as shown in Figure 1a. The unmasked graphene layers were removed by high-density plasma etching using an Ar (89%) and O₂ (11%) mixture. Ar ions enhanced the etching mechanism by introducing defects into the graphene to create starting points for oxidation.^[10,11] The PMMA mask was dissolved using acetone. A 100 nm thick AlN buffer layer was then deposited onto the patterned graphene/6H–SiC surface, followed by the deposition of ≈ 300 nm thick Al_{0.2}Ga_{0.8}N and ≈ 1.5 μm thick GaN layers, as shown in Figure 1b.

2.2. Microstructure and Crystallographic Orientation Relationship

A preliminary visual check of the sample surface revealed a periodic pattern of lines, indicating irregular nitride growth. Figure 1c shows a scanning electron microscopy (SEM) image

of the surface of the GaN. The dark spots, which are inversion domains in the GaN, are present in lines of 1 μm width and 3 μm spacing. By comparing the dimensions of the inversion domain regions with the geometry of the graphene patterning and etching, it is evident that the smooth GaN regions without inversion domains form above the graphene layers. However, as shown below, the etching process does not remove the graphene layers from the SiC perfectly, but leaves islands. The AlN grains then start to grow directly on the SiC and overgrow the graphene islands. Based on the SEM image shown in Figure 1c, the inversion domain density is determined to be 3×10^8 cm⁻².

In order to study the growth of the heterostructure, the sample was analyzed in cross-sectional geometry. Figure 1d shows a low-magnification bright-field (BF) TEM image of a cross-sectional sample of the heterostructure. The GaN layer can be seen to contain semicircular polycrystalline regions above the intact graphene layers. In Figure 1d, the straight vertical dark lines are inversion domains, which travel straight to the surface from regions where the AlN/GaN grows directly on the SiC. By estimating the specimen thickness using electron energy-loss spectroscopy (EELS) to be between 80 and 120 nm for the region shown in Figure 1d, the dislocation density was determined to be $\approx 3 \times 10^9$ cm⁻². A control sample without graphene layers (see Supporting Information) was grown

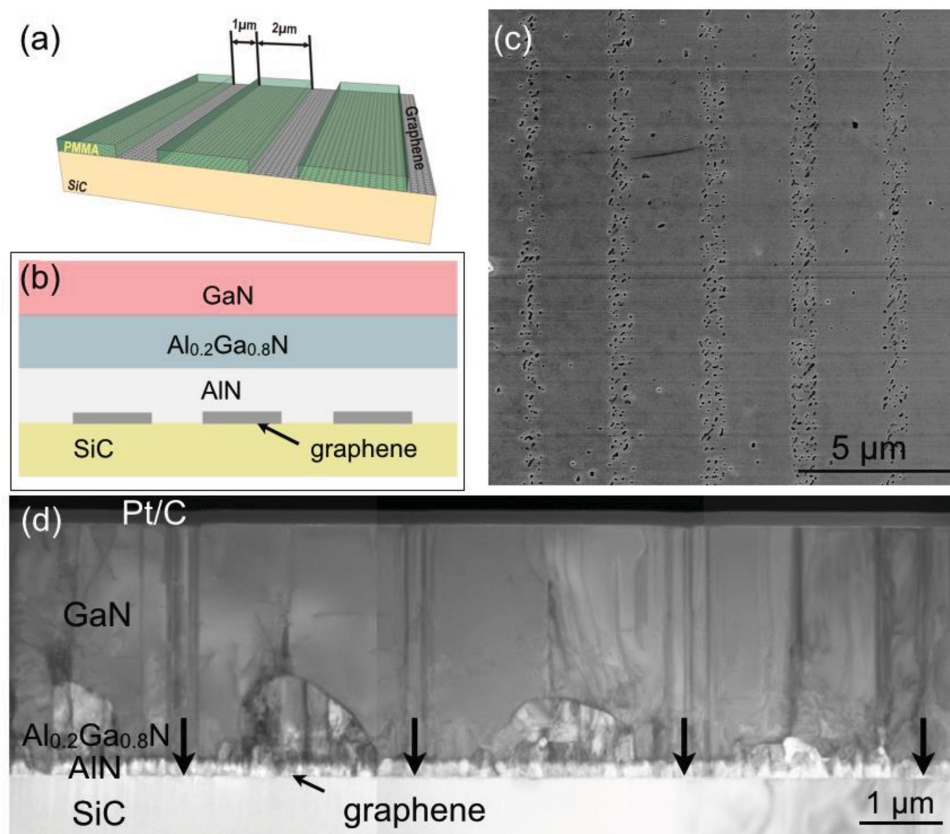


Figure 1. a) Schematic illustration of graphene layers patterned using PMMA. b) Schematic diagram showing the deposited layer sequence. c) SEM secondary electron image of the surface of the final heterostructure grown on the patterned graphene layers. The dark spots are inversion domains in the GaN layer. d) Low-magnification bright-field TEM image of the heterostructure. Arrows mark the regions where the graphene layers were partially etched away in 1 μm wide regions. The Pt/C is a protective layer deposited during specimen preparation to prevent Ga-ion implantation. The specimen thickness is ≈ 100 nm.

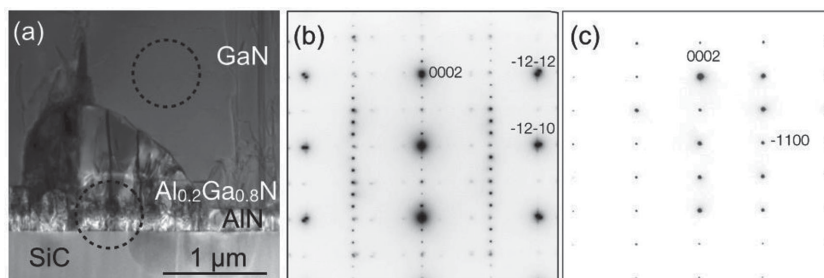


Figure 2. a) BF TEM image showing the transition region close to the substrate, where single-crystalline GaN laterally overgrows the defective GaN that forms above the graphene layers. The dashed circles in (a) indicate the regions that were used to record SAED patterns from b) the substrate, AlN, $\text{Al}_{0.2}\text{Ga}_{0.8}\text{N}$ and defective GaN and c) the single-crystalline GaN.

using identical parameters and had a dislocation density of $2 \times 10^9 \text{ cm}^{-2}$.

The cross-sectional view shown in Figure 1d reveals half-circle-shaped defective regions in the GaN, in which many grain boundaries are present. The microstructure of GaN around this defective region was studied using BF TEM images and selected area electron diffraction (SAED) patterns, as shown in Figure 2. The SAED pattern shown in Figure 2b was recorded from a region that overlapped the substrate and the defective region containing the AlN and GaN layers, as marked by the lower circle in Figure 2a. The AlN on the graphene layers is epitaxial with the SiC substrate, according to the relationship $[11\bar{2}0]_{\text{AlN}}(0002)_{\text{AlN}}/[10\bar{1}0]_{\text{SiC}}(0002)_{\text{SiC}}$. The splitting of the $[-12\bar{1}2]$ reflection in Figure 2b results from the epitaxial growth of GaN on AlN. Interestingly, the GaN layer above the defective region has a $[10\bar{1}0]$ orientation, which is different from the $[11\bar{2}0]$ orientation observed outside the defective region. The overgrown GaN layer is, therefore, rotated by 30° relative to the defective region.

2.3. Chemically Sensitive Imaging of the Interfaces

Compositionally sensitive high-angle annular dark-field (HAADF) scanning TEM (STEM) revealed the formation of a superlattice of AlN and GaN layers in the 300 nm thick $\text{Al}_{0.2}\text{Ga}_{0.8}\text{N}$, as shown in Figure 3, in which the contrast variations reflect the atomic number differences between Al ($Z = 13$) and Ga ($Z = 31$) in the nitride layers. Figure 3a shows an HAADF STEM image recorded from a region close to the substrate. The AlN surface is rough, with grain height differences of between 50 and 200 nm. The arrows indicate superlattice regions, which grow ≈ 500 nm into the GaN layer. The superlattice regions begin on the AlN grains where an $\text{Al}_{0.2}\text{Ga}_{0.8}\text{N}$ layer was supposed to grow according to the growth procedure. Figure 3b,c show magnified images of the AlN/GaN superlattices. Close to the GaN layer, the GaN layer thickness in the superlattice decreases from ≈ 10 to ≈ 4 nm. The high-resolution HAADF STEM image of the superlattice shown in Figure 3c was acquired from a region where the AlN is approximately four monolayers thick. The AlN and GaN layers are in perfect epitaxy, with no evidence of planar defects. Mohseni et al.^[12] observed phase separation in InGaAs nanowires grown on graphene and described it as a special case of van der Waals

epitaxy. In our experiments, the $\text{Al}_{0.2}\text{Ga}_{0.8}\text{N}$ layer did not grow directly on the graphene layers and so the phase separation cannot be explained in the same way. The superlattice formation mechanism is not understood at present, but is thought to be related to the growth of the nitride layers on graphene. Although C contamination could inhibit phase pure $\text{Al}_{0.2}\text{Ga}_{0.8}\text{N}$ layer growth, high-resolution compositional experiments using energy-dispersive X-ray spectroscopy and EELS were not able to reveal C enrichment at the interfaces between the AlN and GaN layers. However, the measurement of small C concentration differences is very challenging

using TEM, especially as the high-energy electron beam can deposit C onto the surface of the specimen. In order to further elucidate the mechanism of AlN/GaN superlattice formation, a control sample grown without graphene layers using an identical procedure was also studied (see Supporting Information). An AlN/GaN superlattice was not observed in the latter sample, suggesting that the phase separation may indeed originate from the presence of C during layer growth.

The growth of AlN grains on intact and etched graphene layers was also studied using high-resolution HAADF STEM. Figure 4 shows HAADF STEM and BF STEM images recorded simultaneously from the interfacial regions, providing information about both the formation of graphene layers on 6H-SiC

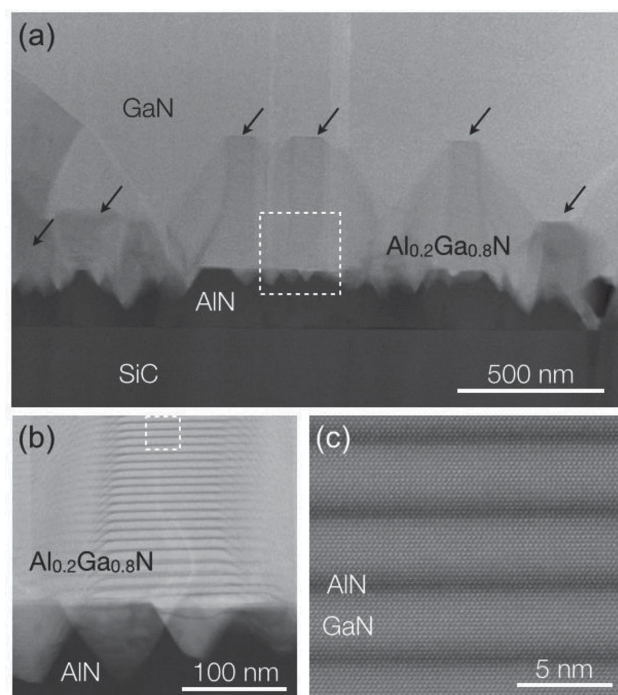


Figure 3. a) STEM HAADF images of the AlN/GaN superlattices, which are marked with arrows. The inner ADF detector semiangle used was 78 mrad. The dashed rectangles in (a) and in (b) indicate the regions shown in (b) and (c), respectively. In (b), the AlN and GaN layer periodicity decreases in the growth direction. The atomic-resolution HAADF STEM image in (c) shows sharp interfaces, with an AlN layer thickness of ≈ 1 nm.

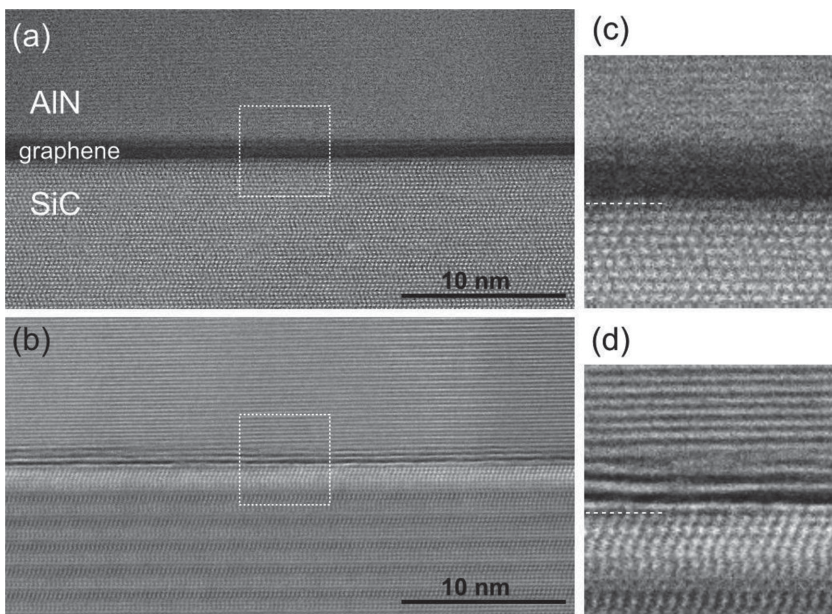


Figure 4. Atomic-resolution a) HAADF STEM and b) BF STEM images of AlN grown on non-etched graphene layers. The regions marked by dashed rectangles in (a) and (b) are enlarged in (c) and (d), respectively. The graphene layers, Al and Si columns appear bright in the HAADF STEM images and dark in the BF STEM images. The uppermost SiC layer is marked by a dotted line. The inner ADF detector semi-angle used was 78 mrad.

and the growth of AlN on graphene. The AlN grain is observed to grow on three graphene layers. The image intensity of HAADF STEM, I depends from atomic number, $\approx Z^{1.7}$ that

results in a lower contrast of carbon than of Al and Si atomic columns. In order to find the location of the graphene layers, BF STEM image is also shown in Figure 4b. The origin of the bright contrast in the uppermost SiC layers visible in Figure 4b is not understood at present, but may be associated with compositional variations or strain. Yu et al.^[13] showed that the presence of strain at a SiO₂/Si interface results in a change in ADF STEM image intensity, which depends on inner detector semiangle and specimen thickness. However, the high-temperature annealing of 6H-SiC that was used to prepare the graphene layers may also have led to a slightly off-stoichiometric composition in the last few layers of the 6H-SiC, with Si diffusing out. The sharp interface between the AlN grain and the graphene layers shows that the PMMA layer was removed completely and that the AlN grew directly on the graphene.

As described above, Ar/O₂ plasma etching was used to remove the graphene layers in stripes from the SiC surface. **Figure 5** shows high-resolution BF and HAADF STEM images of AlN growth on a graphene island that remained on the etched surface of the

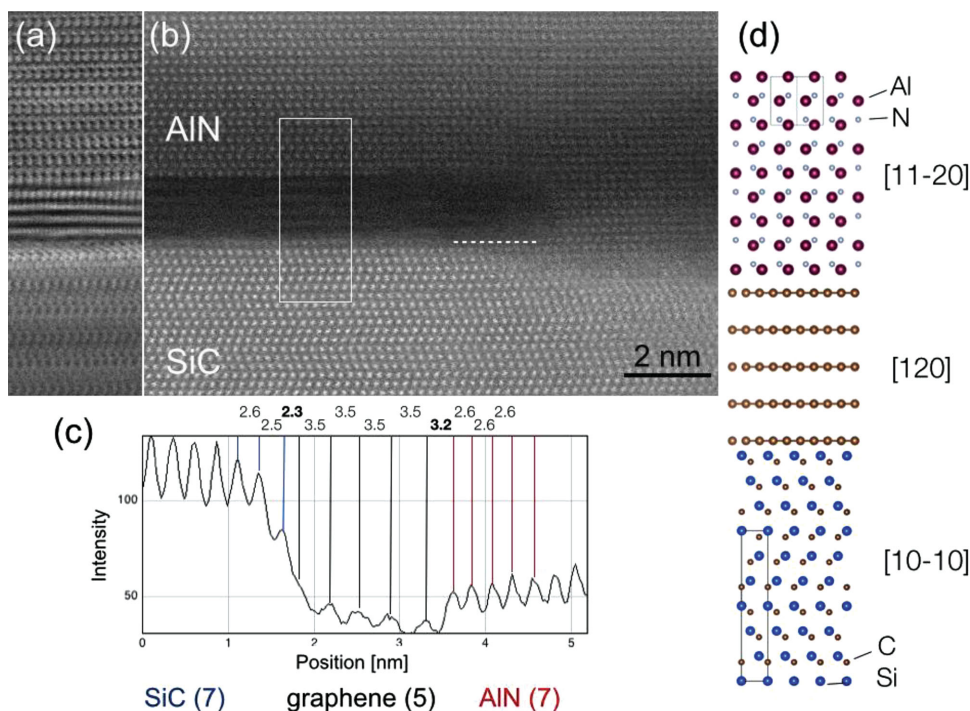


Figure 5. High-resolution aberration-corrected a) BF STEM and b) HAADF STEM images of an etched graphene/AlN interface. Dashed line marks the uppermost Si-C layer. The inner ADF detector semiangle used was 78 mrad. b) Integrated intensity scan across the interface with peak-to-peak distances recorded from the region marked by rectangle in (b). c) Proposed atomistic model of the interface deduced from the STEM images shown in (a, b).

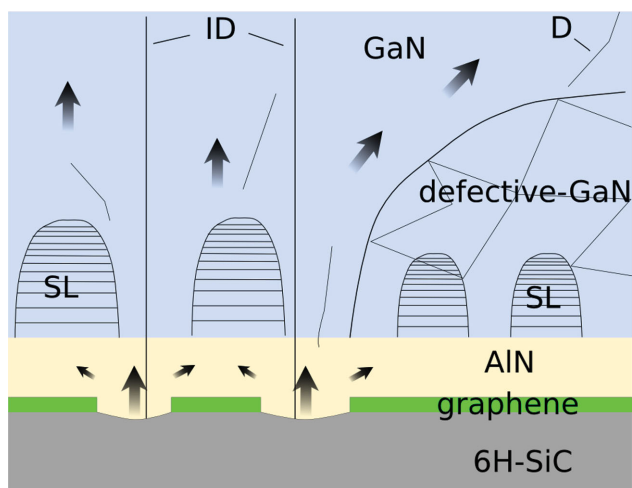


Figure 6. Growth of the nitride heterostructure on etched graphene layers inferred from the present experimental results. SL: GaN/AlN superlattice; ID: inversion domain; D: dislocation. Arrows indicate the growth direction.

spots in Figure 5b are likely to correspond to atomic columns of Si and Al in the 6H-SiC and AlN layers, respectively. Based on the contrast, five carbon layers are thought to be present. On the right side of the image, the graphene layers have been etched away completely and the AlN grains have nucleated directly on the 6H-SiC. The white-dashed line in Figure 5b indicates the uppermost SiC layer. The AlN grain starts to grow below the dashed line, indicating that the etching process also removed ≈ 1 nm of the 6H-SiC. The image suggests that the AlN nucleated and started to grow on the 6H-SiC and then overgrew the graphene layers. Figure 5c shows integrated intensity lines scan obtained across the SiC, graphene and AlN, with the well-defined peaks corresponding to Si, C, and Al layers. Peak-to-peak distances of 2.6 ± 0.1 Å for the 6H-SiC and AlN layers match well with values from the literature for 0002 lattice plane distances of 2.51 Å for 6H-SiC and 2.59 Å for AlN. For the graphene layers, the measured distance between the peaks is 3.5 ± 0.1 Å, which is slightly higher than the expected value of 3.35 Å for graphite. The first carbon layer grown on SiC is the strongly bound buffer layer^[14–17] at the interface that is separated from the uppermost SiC by 2.3 Å. This layer separation matches with values measured by other groups for graphene grown on 4H-SiC(0001)^[18] and 6H-SiC(0001).^[19] Figure 5b,c also show that the intensity of the uppermost Si-C layer is lower and its structure is less defined than that of Si columns in the 6H-SiC, suggesting a nonstoichiometric composition. The AlN grain and graphene are separated by a peak-to-peak separation of ≈ 3.2 Å in Figure 5a. Figure 5c shows an atomic model of the AlN/graphene/Si-C/6H-SiC structure deduced from the high-resolution BF and HAADF STEM images.

3. Summary and Conclusions

Figure 6 shows a summary of the nitride heterostructure growth on graphene layers inferred from the present TEM results. Ar/O₂ plasma etching creates graphene islands on the

6H-SiC substrate and removes the uppermost monolayers of SiC. The AlN nucleates epitaxially on the SiC. The AlN above the graphene layers has the same orientation as the epitaxial AlN on SiC, suggesting that AlN overgrows graphene islands laterally. In the control sample grown without graphene layers, the AlN buffer layer and Al_{0.2}Ga_{0.8}N transition layer were clearly separated and created a sharp interface (see Supporting Information). In contrast to the control sample, the AlN surface on graphene is rough and an AlN/GaN superlattice forms in the Al_{0.2}Ga_{0.8}N transition layers, perhaps as a result of the presence of a small amount of carbon contamination originating from the graphene layers. It is striking that the GaN layer is defective above the intact graphene layers, with a crystallographic orientation that is different from that of the single crystalline GaN above the graphene islands. Inversion domains are found above the etched regions, where the nitride layers grow on SiC. The single-crystalline GaN overgrows the polycrystalline GaN by self-assisted lateral epitaxial overgrowth, reducing the dislocation density and leading to a smooth GaN surface.

We have demonstrated the growth of high-quality GaN layers on etched graphene using an AlN buffer layer and an Al_{0.2}Ga_{0.8}N transition layer. The use of plasma etching of graphene layers in the form of regular stripes leaves islands of graphene, next to which AlN grains nucleate by standard epitaxy on SiC. Polycrystalline GaN forms above the intact graphene layers, which act as a buffer for self-assisted epitaxial lateral overgrowth of a single-crystalline GaN layer. The resulting lateral growth reduces the defect density in the GaN. Inversion domains are found in the regions that form directly on the SiC. The probable presence of C contamination during growth of the Al_{0.2}Ga_{0.8}N transition layer results in the growth of a phase-separated AlN/GaN multilayer, which is not understood in detail at present.

Our results clearly show that nitride heterostructures deposited on patterned graphene layers are grown via lateral overgrowth, which results in the formation of a single-crystalline GaN layer that has a relatively low defect density and a smooth surface. Optimization of the plasma etching process and growth procedure promises to offer a simple route to produce nitride-based device structures with better thermal management due to graphene layer incorporation.

4. Experimental Section

TEM Specimen Preparation: A ≈ 15 μm long thin section was cut out using a dual-beam focused ion beam (FIB) system using ion energies of 30 and 5 keV. A Pt/C protective layer was deposited onto the surface of the GaN using the electron and ion beams with thicknesses of 0.5 and 2.5 μm, respectively. The FIB lamella was fixed onto a standard Cu Omniprobe grid using Pt/C layer deposition. The ion beam-induced surface damage was then reduced by using low-energy (0.5 keV) focused Ar-ion milling at an incident angle of 10° in a Fischione Nanomill 1040 system.

TEM Characterization: For conventional TEM studies, an FEI Tecnai G2 microscope was used at an accelerating voltage of 200 kV. For high-resolution STEM studies, a probe-aberration-corrected FEI Titan 80–300 microscope was used at an accelerating voltage of 300 kV, with the aberration coefficients of the probe forming system corrected to fourth order.

Acknowledgements

The Hungarian National Scientific Research Fund (OTKA) supported this work through Grant No. K108869. The authors acknowledge financial support from the European Union under the Seventh Framework Program under a contract for an Integrated Infrastructure Initiative. Reference 312483 – ESTEEM2. The authors would like to thank D. Meertens (Forschungszentrum Jülich, PGI-5) for the preparation of FIB lamellas. R.Y. acknowledges financial support from the Swedish NRC (VR).

Received: May 8, 2014

Revised: November 15, 2014

Published online:

-
- [1] K. S. Novoselov, V. I. Falko, L. Colombo, P. R. Gellert, M. G. Schwab, K. A. Kim, *Nature* **2012**, 490, 192.
- [2] A. A. Balandin, *Nat. Mater.* **2011**, 10, 569.
- [3] R. J. Trew, D. S. Green, J. B. Shealy, *IEEE Microwave Mag.* **2009**, 10, 116.
- [4] M. H. Crawford, *IEEE J. Sel. Top. Quantum Electron.* **2009**, 15, 1028.
- [5] N. Han, T. V. Cuong, M. Han, B. D. Ryu, S. Chandramohan, J. B. Park, J. H. Kang, Y. J. Park, K. B. Ko, H. Y. Kim, J. H. Ryu, Y. S. Katharria, C. J. Choi, C. H. Hong, *Nat. Commun.* **2013**, 4, 1452.
- [6] K. Chung, K.C.-H. Lee, G. C. Yi, *Science* **2010**, 330, 655.
- [7] Z. Yan, G. Liu, J. M. Khan, A. A. Balandin, *Nat. Commun.* **2012**, 3, 827.
- [8] C. Virojanadara, M. Syväjarvi, A. A. Zakharov, T. Balasubramanian, R. Yakimova, L. I. Johansson, *Phys. Rev. B* **2008**, 78, 245403.
- [9] L. Kotis, S. Gurban, B. Pecz, M. Menyhard, R. Yakimova, *Appl. Surf. Sci.* **2014**, 316, 301.
- [10] J. S. Moon, D. Curtis, S Bui, M. Hu, D. K. Gaskill, J. L. Tedesco, P. Asbeck, G. G. Jernigan, B. L. VanMil, R. L. Myers-Ward, C. R. Eddy, P. M. Campbell, X. Weng, *IEEE Electron Device Lett.* **2010**, 31, 260.
- [11] P. L. Neumann, E. Tóvári, S. Csonka, K. Kamarás, Z. E. Horváth, L. P. Biró, *Nucl. Instrum. Methods Phys. Res. B* **2012**, 282, 130.
- [12] P. K. Mohseni, A. Behnan, J. D. Wood, C. D. English, J. W. Lyding, E. Pop, X. Li, *Nano Lett.* **2013**, 13, 1153.
- [13] Z. Yu, D. A. Muller, J. Silcox, *J. Appl. Phys.* **2010**, 95, 3362.
- [14] W. A. de Heer, C. Berger, M. Ruan, M. Sprinkle, X. Li, Y. Hu, B. Zhang, J. Hankinson, E. Conrad, *Proc. Natl. Acad. Sci. USA* **2011**, 108, 16900.
- [15] C. Virojanadara, R. Yakimova, A. A. Zakharov, L. I. Johansson, *J. Phys. D: Appl. Phys.* **2010**, 43, 374010.
- [16] K. V. Emtsev, F. Speck, T. Seyller, L. Ley, J. D. Riley, *Phys. Rev B* **2008**, 77, 155303.
- [17] L. H. de Lima, A. de Siervo, R. Landers, G. A. Viana, *Phys. Rev. B* **2013**, 87, 081403(R).
- [18] J. Borysiuk, W. Strupirski, R. Božek, A. Wyszomolek, J. M. Baranowski, *Mater. Sci. Forum* **2009**, 207, 615.
- [19] W. Norimatsu, M. Kusunoki, *Chem. Phys. Lett.* **2009**, 468, 54.
-